Hindawi
Advances in Civil Engineering
Volume 2019, Article ID 9276839, 12 pages
https://doi.org/10.1155/2019/9276839

Research Article

Structural Behavior of Ultrahigh-Performance Fiber-Reinforced Concrete Thin-Walled Arch Subjected to Asymmetric Load

Jun Yang[1], **Jianting Zhou**[1,2], **Zongshan Wang**[1], **Yingxin Zhou**[3] **and Hong Zhang**[1]

[1]*School of Civil Engineering, Chongqing Jiaotong University, Chongqing 400074, China*
[2]*State Key Laboratory Breeding Base of Mountain Bridge and Tunnel Engineering, Chongqing 400074, China*
[3]*Yunnan Wuyi Expressway Construction Command, Kunming 650000, China*

Correspondence should be addressed to Jianting Zhou; jtzhou@cqjtu.edu.cn

Received 28 November 2018; Accepted 30 January 2019; Published 18 February 2019

Academic Editor: Eric Lui

Ultrahigh-performance fiber-reinforced concrete (UHPFRC) is an innovative material in the field of bridge engineering. With superior mechanical characteristics, this new material reduced the structural self-weight and extended the span of modern bridges. A series of tests should be conducted to establish reliable design rules for UHPFRC structures. This paper aimed at determining the compressive behavior of UHPFRC for thin-walled arch section design and a comparison was made with a normal concrete (NC) arch. Eighteen axial compression columns for arch section design and arches under asymmetric load were tested in this paper. Behaviors of the arches were assessed using various mechanical properties, including the failure pattern, load-deflection relationship, strain analysis, and analytical investigation. A finite element model (FEM) considering the material and geometric nonlinearity was developed to predict the behavior of the UHPFRC arch. Results indicated that a wall thickness of 50 mm with stirrups effectively restrained instability failure of the thin-walled compression columns. The cracking load and the ultimate load of the UHPFRC arch increased by 60% and 34%, respectively, when comparing with the NC arch. It showed the UHPFRC arch had higher load capacity and outstanding durability. The failure mode of the UHPFRC arch was similar to that of the NC arch, which belonging to the destruction of multihinges. However, the appearance of the plastic hinges was delayed, and a better elastic-plastic performance was obtained when using UHPFRC. The analytical formula for calculating the ultimate load of the UHPFRC arch was derived with high precision by using the limit equilibrium method. The results of the FEM showed good agreement with test results, and they were able to predict the behavior of the UHPFRC arches.

1. Introduction

After years of research and practice, ultrahigh-performance fiber-reinforced concrete (UHPFRC) has made its way into the construction field. UHPFRC is a cement-based and hybrid fiber composite material with ultrahigh mechanical performance that can reduce structure sectional size and make structures more lightweight, so it is widely applied in bridge engineering [1–4]. The main idea is using UHPFRC to build bridges where structures are mainly subjected to high mechanical loading [5], high seismic zones [6], and severe environment [7]. There have been some successful UHPFRC bridge constructions, and UHPFRC is used as major or part of building materials.

Several recent studies have focused on UHPFRC beam structures [8, 9]. Different kinds of novel and unprecedented lightweight beam bridges are developed by engineering researchers [10], and various strengthening techniques with UHPFRC are used for existing reinforced concrete beam bridges [11–14]. However, the most significant mechanical properties of UHPFRC are high compressive strength and flexural strength. Li et al. studied the postblast capacity of UHPFRC columns, and the test results revealed that UHPFRC columns retained most of their loading capacity after blast loads [15]. This feature makes UHPFRC very suitable for compressed members. Studies on UHPFRC columns have mainly concentrated on solid section. Adnan and Stephen investigated six UHPFRC columns without

steel ties, and the results indicated high volumes of steel fibers can prevent both spalling of cover concrete and buckling of longitudinal rebars [16]. Shi et al. considered the influences of section dimension of the columns, reinforcement ratio, and steel fiber, tested the behavior of twenty-two UHPFRC columns under eccentric compression, and found the section thickness has the most significant influence on the bearing capacity [17]. Hung et al. experimentally investigated the slender UHPFRC columns under eccentric loading. It was found that the inclusion of a 1.5% volume fraction of steel fibers was able to compensate a 70% reduction in the confinement steel, and the ductility of the UHPFRC columns was promoted [18]. Muhammad and Ahmed analyzed the influence of steel fibers inclusion on the behavior of UHPFRC columns under eccentric and four-point bending. The outcomes showed the hybridization between macrofiber and deformed fiber resulted in better ductility compared to only one kind of steel fiber addition or no fiber [19].

UHPFRC compared to normal concrete (NC) without steel fibers has significantly higher strength and toughness. It can be successfully used for thin-walled members, but there are few experimental studies about the compressive strength of thin-walled components. Shan et al. tested the compressive UHPFRC tubes with a thickness of 20 mm. The experiments showed that axial load carrying capacity of UHPFRC thin-walled columns was controlled by stability instead of material strength, and it was only 48% of the ultimate strength of material [20]. The stability is the primary problem that should be considered in the design of UHPFRC thin-walled arches and columns.

In summary, despite these valuable research works on the bearing characteristic of UHPFRC columns, it can be noted that none of studies consider the relationship between column design and arch structure design. In addition, the structural behavior regarding a comparison of NC for the advantages of UHPFRC arches is still lacking in the literature. It is hard to propose a simple analytical method for designing the UHPFRC column or compressive structures. The objective of this research is to further understand the structural mechanical performance of the UHPFRC arch and make full use of material strength in UHPFRC structural design.

2. Experimental Program

2.1. Materials. The mix proportion of UHPFRC material is summarized in Table 1. In addition, the straight-shaped steel fibers with a diameter of 0.12 mm and a length of 8 mm and with a tensile strength of 2200 MPa were mixed. The volume percentage of steel fibers was fixed at 2%.

According to Chinese codes, code for reactive powder concrete (GB/T31387-2015) and code for design of concrete structures (GB50010-2010), compressive strength and flexural strength tests were conducted on 100 mm cubes and $100 \times 100 \times 400\ mm^3$ prisms, respectively. $100 \times 100 \times 300\ mm^3$ prisms were prepared for measuring the elastic modulus. The ratio of compressive strength f_c and cube compressive strength f_{cu} was 0.82 in accordance with GB50010-2010, and the testing results are shown in Table 2. The columns were reinforced with D6 and D4 HRB335 rebars that had a nominal yield strength of 335 MPa. Both the D6 and D4 bars were having a test yield stress of 427 MPa, and the ultimate strengths of 539 MPa and 520 MPa, respectively. Both bars had the same elastic modulus of 215 GPa.

2.2. Strength Properties of UHPFRC Columns. Because there were no existing design guidelines for UHPFRC arch design, in this section, the axial compressive tests were performed on eighteen UHPFRC columns to determine the reasonable and economic section for UHPFRC arches. The notations and details of the columns are summarized in Table 3. The columns had a total height of 800 mm; an outer cross section of $200 \times 200\ mm^2$; the wall thickness of 30 mm in group A and 50 mm in group B; and the stirrup spacing of 50 mm, 100 mm, and unmatched stirrups.

Solid sections were designed at the two ends of the columns to limit the local damage caused by local buckling. The demolding of all columns occurred 24 h after casting. The curing treatment applied to columns was steam curing for 48 h, and then the columns were tested (Figure 1).

During the test, an axial compressive load was applied to the thin-walled columns using a press with a loading capacity of 5000 kN at a rate of 180 kN/min. The value of the applied vertical force was measured using the electrohydraulic servo system. The deflection of the columns was obtained by using a electronic digital micrometer. When the load reached 90% of ultimate load (Pu), the loading mode was changed to displacement control at a rate of 0.05 mm/min until the specimens were destructed. A test loading device is shown in Figure 2.

The measured ultimate loads of UHPFRC thin-walled columns are given in Figure 3. The material utilization rates reached 70.88%, 75.69%, and 91.27%, respectively, in groups A1 to A3, and the rates were 87.65%, 95.50%, and 95.12% in groups B1 to B3. It can be seen that the design of a thin wall and lack of stirrups resulted in premature failure. Stirrups enhanced structural stability, but too much stirrups had no contribution to structural strength.

The section in group B2 was selected by reliability and economy for the UHPFRC arch design. High strength and high toughness of material performance could be fully used in UHPFRC thin-walled section with the thickness of 50 mm and a reasonable number of stirrups.

2.3. Arch Specimen Details and Test Procedures. UHPFRC and NC arches had the same dimensions. The tested arches (as shown in Figure 4) had a computing span (L) of 2000 mm, the calculated height (f) of 500 mm, span ratio of 1/4, and arch axis equation of $y = (4f/L)x(1 - x/L)$. The section was the same as columns in group B2. Diaphragms with a thickness of 40 mm at both sides of arch feet, 3L/4 and L/2, and the thickness of 80 mm at the loading point (L/4) were designed to prevent local damage. The prefabricated arches were bonded to steel arch abutment using epoxy adhesive.

Table 1: UHPFRC mix proportion.

Components	Cement	Silica fume	Quartz sand	Quartz flour	Water reducer	Water
Mass ratio	1.000	0.250	1.100	0.300	0.019	0.225

Table 2: Measured mechanical properties of UHPFRC.

Material	Cube compressive strength (MPa)	Compressive strength (MPa)	Bending strength (MPa)	Elastic modulus (GPa)	Poisson's ratio
UHPFRC	140	115	28	43	0.19

Table 3: Parameters of the tested column specimens.

Group	Column	Wall thickness (mm)	Longitudinal rebar	Ratio of rebar (%)	Stirrup	Quantity of specimen
A1	B30S000	30	None	0	None	3
A2	B30S100	30	4D6	0.55	D4@100 mm	3
A3	B30S050	30	4D6	0.55	D4@50 mm	3
B1	B50S000	50	None	0	None	3
B2	B50S100	50	4D6	0.38	D4@100 mm	3
B3	B50S050	50	4D6	0.38	D4@50 mm	3

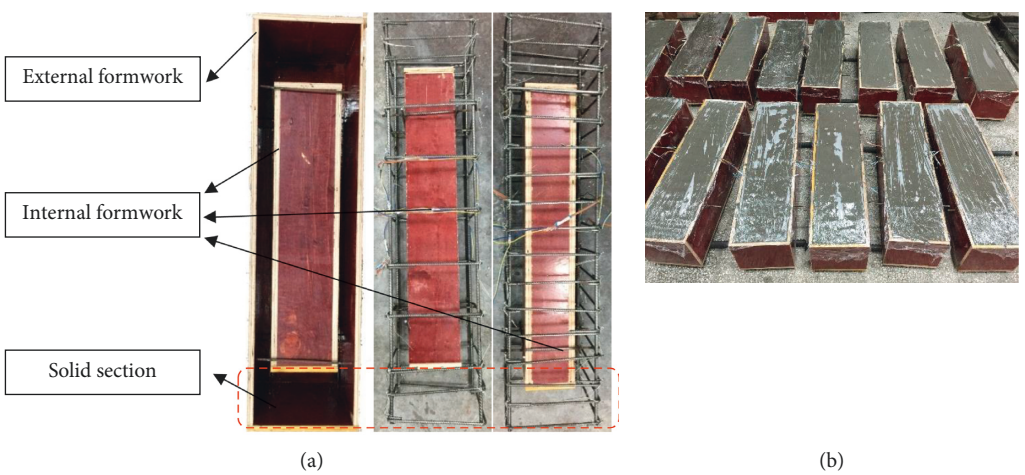

Figure 1: Specimen details. (a) Formwork creation and installation. (b) UHPFRC casting.

Figure 2: Experimental setup of columns.

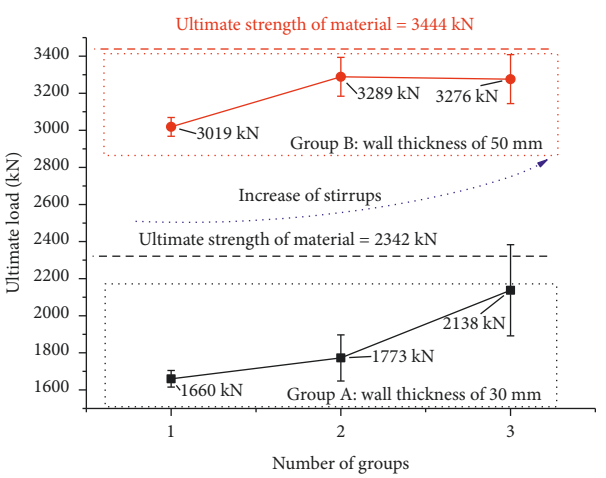

Figure 3: Ultimate loads of columns.

Figure 4: Test scheme and instrumentation of the arch test.

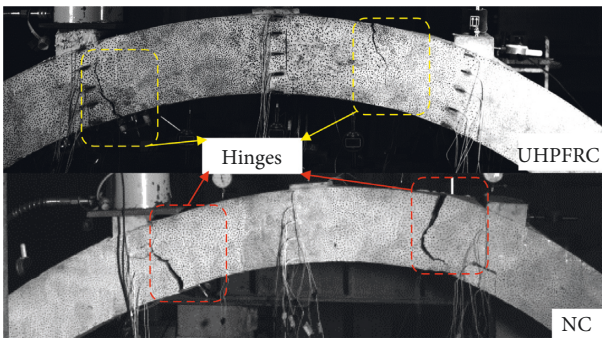

Figure 5: Failure patterns for UHPFRC and NC arches.

The arches carried an asymmetric concentrated load at L/4 section. The strain, crack distribution, and vertical and lateral displacement under different loading conditions, as well as the cracking load and ultimate load, were recorded.

3. Experimental Results and Discussion

3.1. Failure Characteristics and Cracks. Tests of the failure characteristics and cracks of the UHPFRC arch and NC arch were performed. Both the UHPFRC and NC arches failed by multihinges collapse mode, as shown in Figure 5. The tests showed that many tightly spaced cracks formed near the main cracks, and the appearance of plastic hinges in the UHPFRC arch was much later than those in the NC arch. These results indicated the UHPFRC arch had a better crack dispersive ability and underwent multiple cracking before failure. These patterns were different from the typical failure pattern of the NC arch.

Tests of the propagation of main cracks were performed at each loading step as shown in Figure 6. The first crack occurred at the bottom slab of L/4 section. The first cracking loads of UHPFRC and NC arches were 40 kN and 25 kN, respectively. The cracking load of the UHPFRC arch is 60% more than that of the NC arch. The Pu of the UHPFRC arch was 390 kN, and it was higher than that of the NC arch by 34%. Before the load reached 56% Pu, the crack width was less than 0.05 mm in the UHPFRC arch. The microcracks had no significant effect on structural durability [21]. Therefore, the UHPFRC arch had higher load capacity and outstanding durability.

3.2. Load-Deflection Behavior. During the test, the lateral maximum displacements at L/4, L/2, and 3L/4 were 1.27 mm, 0.881 mm, and 0.430 mm, respectively. Therefore, the UHPFRC arch was considered under in-plane loads. The horizontal displacements of the steel arch abutment were 0.750 mm and 0.610 mm, respectively. The steel arch abutments remained stable.

The relationships between the cross-sectional load and the deflection of the seven key points of the arch were plotted (Figure 7). The vertical deformations of all sections increased linearly with the increase in load before yielding of tension steels, and the arch stiffness remained unchanged before the initial cracking at 40 kN. However, with the increase in load, the stiffness decreased slightly when cracks spreaded through the section. The steel bars in the bottom were yielded at 190 kN. Thereafter, the sections far from loading section (L/2, 5L/8, 3L/4, and 7L/8) were with upward deformation. The three farther sections (5L/8, 3L/4, and 7L/8) reached the "reversal points" and began to move upward. The test results agreed with the deformation law of arch structure under asymmetric load.

Typical load deformation behavior at L/4 section is plotted in Figure 8. The loading process was divided into four stages, namely, elastic stage, initial elastoplastic stage, enhanced elastoplastic stage, and failure stage. The fibers in UHPFRC provided tensile forces of a magnitude similar to steel bars. As the strains on the tension side increased, the bottom slab was cracked, the tension steels began to work, and the arch was in the initial elastoplastic stage. The section stiffness was high at this two stages even the arch with tiny cracks.

When the load reached 190 kN, the tensile steel bars yielded and the arch entered the enhanced elastic-plastic stage. The section stiffness was decreased nonlinearly, and the relationship between load and vertical deformation was nonlinear at this stage. With the web cracking, the location of the neutral axis moved higher and a plastic hinge was formed at L/4 section. When the load reached 330 kN, the top plate was cracked and the compression steels were yielded. The deformation velocity was accelerated and the cracks width increased continually until it was destroyed at 390 kN. The typical load deformation relationship showed the UHPFRC arch was in a linear elastic state before 49% Pu and structural deformation was very small before 85% Pu.

3.3. Strain Analysis of Loading Section. The measured strain results of L/4 section under different load levels are given in Figure 9. It was observed that the section met the flat section assumption before steel yielding. The initial neutral axis (Center 0) moved lower with increasing amounts of tension effective UHPFRC steel fiber. With the increase in load and crack width, the effective compressive section reduced and neutral axis moved upwards from center 0 to center 1, center 2, and center 3. It was shown that the UHPFRC arch strain distributing was in line with the plane section assumption at different loading stages. This may be attributed to resistance of the high-volume steel fibers in the cement base to tensile forces even after cracking in the UHPFRC arch.

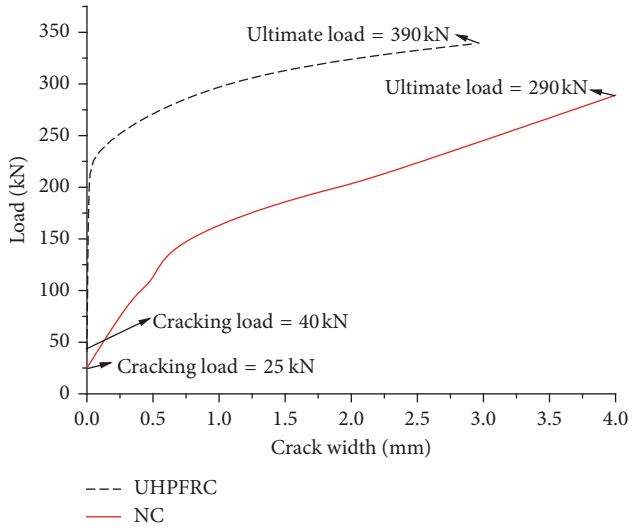

Figure 6: Load versus crack width curves of UHPFRC and NC arches.

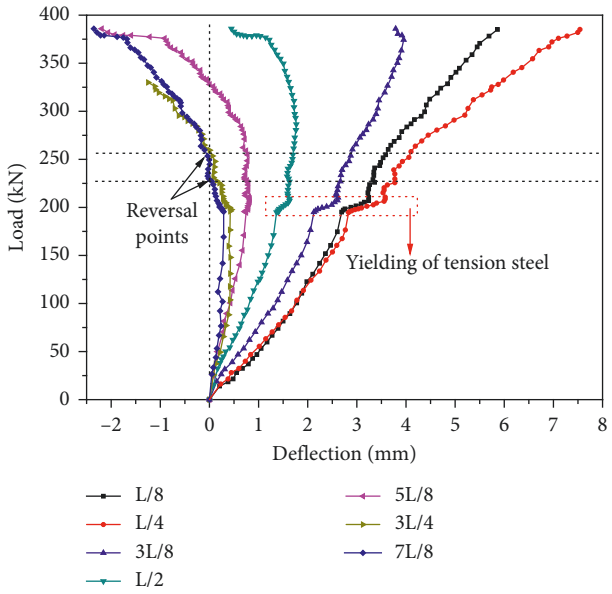

Figure 7: Load-deflection results of key points.

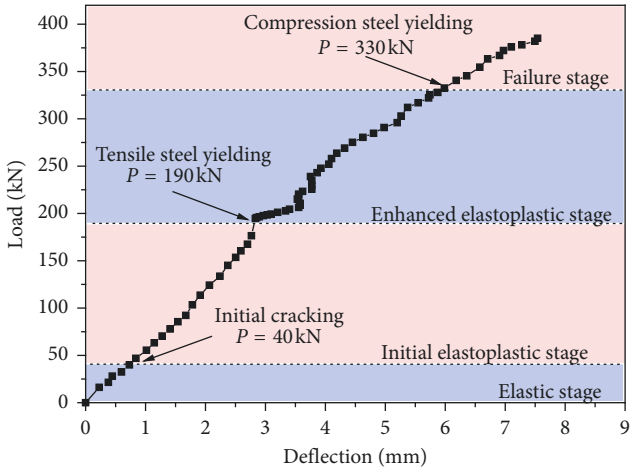

Figure 8: Load-deflection behavior of the L/4 section.

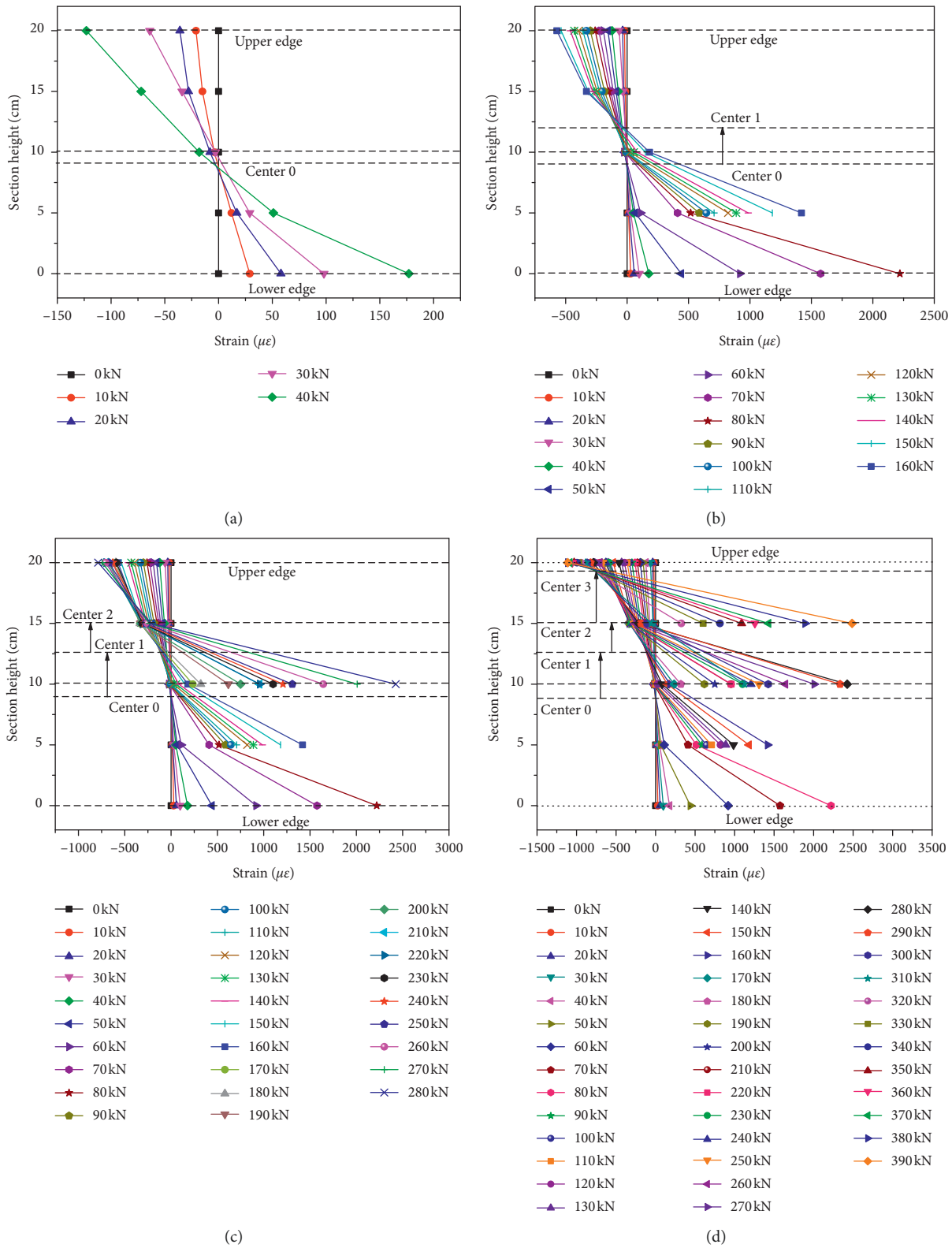

Figure 9: The relationship between section height and strain in different load levels: (a) 0–40 kN; (b) 0–160 kN; (c) 0–280 kN; (d) 0–390 kN.

3.4. Analytical Investigation of UHPFRC Arch. The load capacity of the tested UHPFRC arch was analyzed using a mechanistic model. For the UHPFRC arch structure under small load, the classical elastic theory was adopted, and the internal force and deformation state calculation values of the arch were reliable. However, the testing arch was subjected to

ultimate load, and its internal force and deformation were quite different from the actual situation according to the large stiffness elastic system. Therefore, in the theoretical calculation, the limit equilibrium method was used to analyze [22]. The following conditions were assumed to be satisfied: (1) the internal force distribution of the arch was balanced with the external load; (2) if the number of plastic hinges in the arch reaches four, the arch structure formed a "mechanism" system; and (3) the internal force of any section in the arch did not exceed the section ultimate bearing capacity.

Combined with the test arch failure phenomenon, the force diagram was assumed (A/B/C/D: four sections, Figure 10).

The resultant force in the Y direction is $\sum F_y = 0$, and reactions can be obtained via internal force equilibrium as

$$\begin{aligned} V_A &= (1-\alpha)P, \\ V_B &= \alpha P, \end{aligned} \tag{1}$$

where P is the concentrated load and α is the load position coefficient.

A hinge formed at the loading section (C section), but the position of the other hinge D was unknown. The coordinates of hinges C and D can be assumed as

$$\begin{aligned} &C(x_C, y_C), \\ &D(x_D, y_D). \end{aligned} \tag{2}$$

The arch axis equation can be expressed as

$$\begin{aligned} y &= \beta x\left(1-\frac{x}{L}\right), \\ \beta &= \frac{4f}{L}. \end{aligned} \tag{3}$$

The bending moments of hinges C and D can be written as

$$\begin{aligned} M_C &= V_A x_C - H y_C \\ &= (1-\alpha)P \cdot \alpha L - H \cdot \frac{4f}{L}\alpha L(1-\alpha) \\ &= \alpha L(1-\alpha)(P-\beta), \end{aligned} \tag{4}$$

$$\begin{aligned} M_D &= V_A x_D - P(x_D - x_C) H y_D \\ &= (1-\alpha)P x_D - P(x_D - \alpha L) - H y_D \\ &= P(L - x_D)\alpha - H y_D. \end{aligned} \tag{5}$$

When the moment reached the maximum value, y_D' can be calculated by

$$\begin{cases} \dfrac{dM_D}{dx^2} = 0, \\ -\alpha P - H y_D' = 0, \\ y_D' = -\dfrac{\alpha P}{H}. \end{cases} \tag{6}$$

When multihinges are formed, M_C can be calculated by

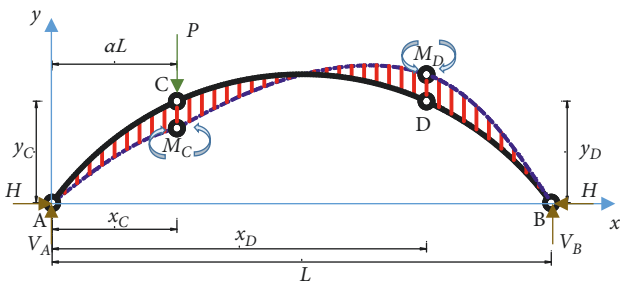

Figure 10: Failure mode of the arch under a concentrated load at L/4.

$$|M_C| = |M_D| = |M_{\text{ultimate}}|, \tag{7}$$

$$M_C = -M_D = |M_{\text{ultimate}}|. \tag{8}$$

When substituted for equations (4) and (5), equation (8) can be expressed as

$$\begin{aligned} \alpha L(1-\alpha)(P - H\beta) &= -[\alpha P(L - x_D) - H y_D], \\ \frac{\alpha P}{H} &= \frac{y_D + \alpha\beta L(1-\alpha)}{L(2-\alpha) - x_D}. \end{aligned} \tag{9}$$

By a direct computation, x_D and H can be derived as

$$x_D = L[\alpha(\sqrt{2} - 1) + (2 - \sqrt{2})], \tag{10}$$

$$H = -\frac{-\alpha P}{\beta[(2\sqrt{2} - 3) - 2(\sqrt{2} - 1)\alpha]}. \tag{11}$$

Equation (10) shows that the location of the plastic hinge has nothing to do with the ratio of the rise to span of the arch but only to the position of the concentrated load.

In this experiment, when substituted $\alpha_s = \alpha_s' = 25$ mm, $L = 2000$ mm, $f = 500$ mm, and $\beta = (4f/L) = 0.5$ into equations (10) and (11), x_D and H can be calculated as follows:

$$\begin{aligned} x_D &= 1379 \text{ mm}, \\ H &= 0.6602P. \end{aligned} \tag{12}$$

The position of hinges C and D can be obtained. The inclination angle between the arch axis and the horizontal axis at C and D can be expressed as follows:

$$\begin{aligned} \tan\varphi_C &= y_C', \\ \tan\varphi_D &= y_D'. \end{aligned} \tag{13}$$

For section C, the internal forces can be expressed as follows:

$$N_C = H\cos\varphi_C + P_P \sin\varphi_C, \tag{14}$$

$$M_C = V_A x_C - H y_C, \tag{15}$$

$$\therefore P_P = P - V_A, \tag{16}$$

where P_P is the vertical forces generated by the concentrated load on the right side of section C.

Substituted equation (16) into (14), the internal forces can be expressed as follows:

$$N_C = 0.7023P, \tag{17}$$

$$M_C = 127.4293P. \tag{18}$$

Form the equation (18), the eccentricity can be calculated as follows (Figure 11):

$$e_0 = \frac{M_C}{N_C} = 181.4472\,\text{mm},$$

$$e = e_0 + \left(\frac{h}{2} - a_s\right) = 256.4472\,\text{mm}, \tag{19}$$

$$e' = e_0 - \left(\frac{h}{2} - a_s'\right) = 106.4472\,\text{mm}.$$

The tension resistance provided by the fibers, f_{fib}, can be obtained as [23]

$$f_{\text{fib}} = \frac{V_{\text{fib}}}{A_{\text{fib}}} \cdot \alpha \cdot \tau\pi d_{\text{fib}} \frac{l_{\text{fib}}}{2}, \tag{20}$$

where V_{fib} is the fiber volume content; A_{fib} is the cross-sectional area of one fiber; α is the orientation factor accounting for the random orientation of the fibers (for three-dimensional fiber, orientation is assumed $1/\pi$); average bond strength τ is assumed to be 10 MPa; and d_{fib} is the diameter, and l_{fib} is the length of one fiber.

From $\sum M = 0$, the equilibrium equation can be expressed as

$$f_{\text{fib}} A_{\text{sf}} e + f_s A_s e - f_s' A_s' e' = f_c b \cdot x\left(e - h_0 + \frac{x}{2}\right). \tag{21}$$

Substituted section and material parameters into equation (21), the neutral axis depth can be calculated as

$$x = 17.5582\,\text{mm}. \tag{22}$$

Because $x < 2a' = 50$ mm, steel compression force is not considered.

Equation (21) can be rewritten as

$$f_{\text{fib}} A_{\text{sf}} e + f_s A_s e = f_c b \cdot x\left(e - h_0 + \frac{x}{2}\right). \tag{23}$$

Neutral axis depth can be recalculated as

$$x = 18.6914\,\text{mm}. \tag{24}$$

From the equilibrium equation $\sum N = 0$, axial force N can be calculated as

$$N = f_c b \cdot x - f_s A_s - f_{\text{fib}} A_{\text{sf}} = 278\,\text{kN}. \tag{25}$$

From equation, N_C can be calculated as

$$N_C = 0.7023P = 278\,\text{kN}. \tag{26}$$

The ultimate load of the experimental arch is $P = 396$ kN.

The procedure for computing the predicted load capacity of the UHPFRC arch is as given in Figure 12.

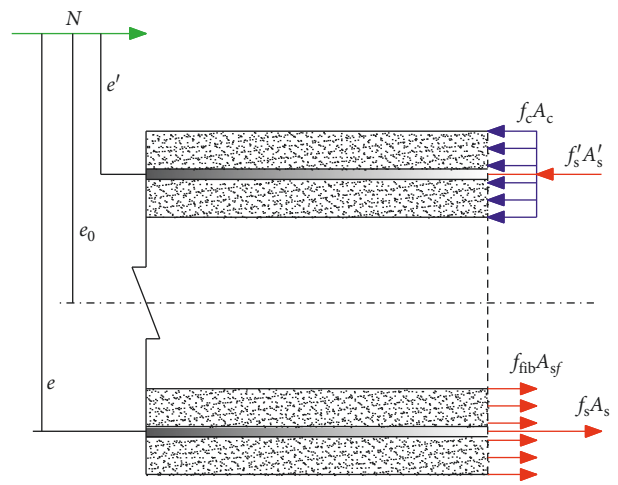

Figure 11: Analytical model.

Results of the load capacity predicted using the analytical model of the arch are compared with those of the experimental test as follows:

$$\frac{P_{\text{Exp}}}{P_{\text{Pre}}} = \frac{390\,\text{kN}}{396\,\text{kN}} = 0.98, \tag{27}$$

where P_{Exp} is the test value and P_{Pre} is the predictive value.

The results showed good agreement for this arch structure.

4. Numerical Investigation

4.1. Material Models and Properties. The constitutive relation of UHPFRC material, combined with the actual test values, a trifold line similar to France [24], Australia [25], Japan [26], and FHWA's research results [27–29] were adopted as shown in Figure 13. The bilinear elastic-plastic constitutive relation was adopted for the steel bar, with the yield stress of 427 MPa, the elastic modulus of 215 GPa, Poisson's ratio of 0.3, and the density of 7800 kg/m^3.

4.2. UHPFRC Arch Modelling

4.2.1. Finite Element Model Establishment. The press-bending behavior of the tested arch was simulated using nonlinear finite element analysis for better understanding of the response and bearing capacity of the UHPFRC arch (Figure 14). The 8-noded hexahedral linear reduction and integration element (C3D8R) was used to model the UHPFRC, and 2-noded linear 3-D truss element (T3D2) was used to model steel bars and stirrups. Assuming perfect bond, the embedded constraint was used to fuse together the steel and UHPFRC.

4.2.2. Calculation Result Analysis. The numerical results of the UHPFRC arch were compared to the crack pattern and load-deflection results of the tested arch, and the results are presented in Figure 15.

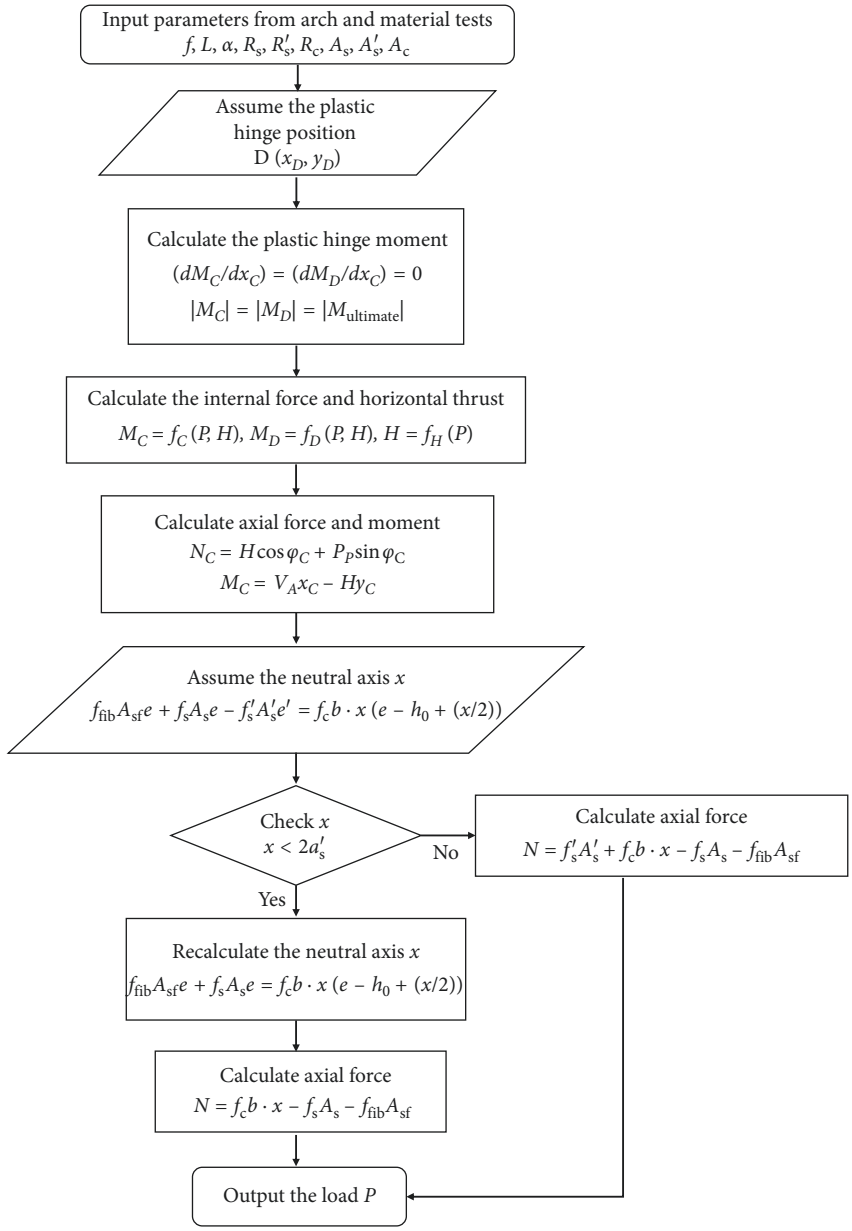

Figure 12: Flowchart for the analytical model.

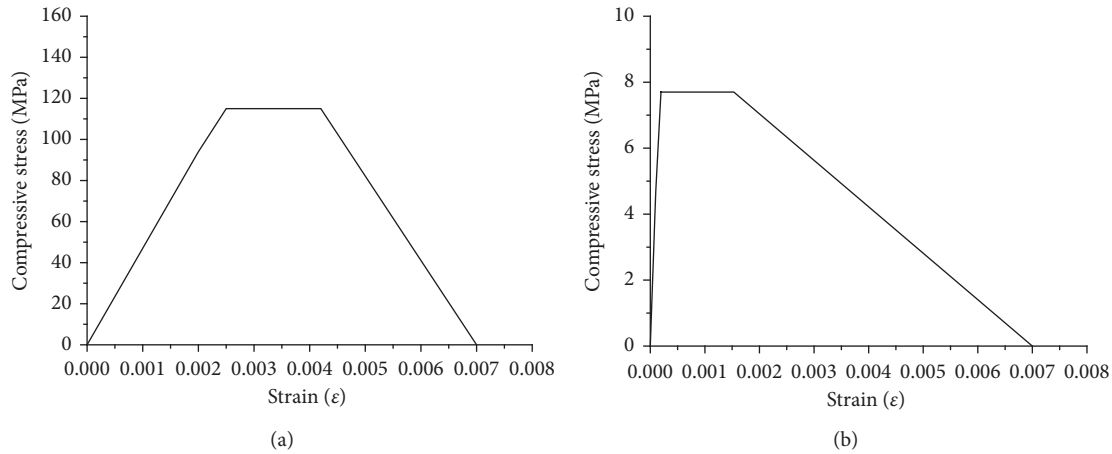

Figure 13: Stress-strain curve of UHPFRC under (a) uniaxial compression and (b) uniaxial tension.

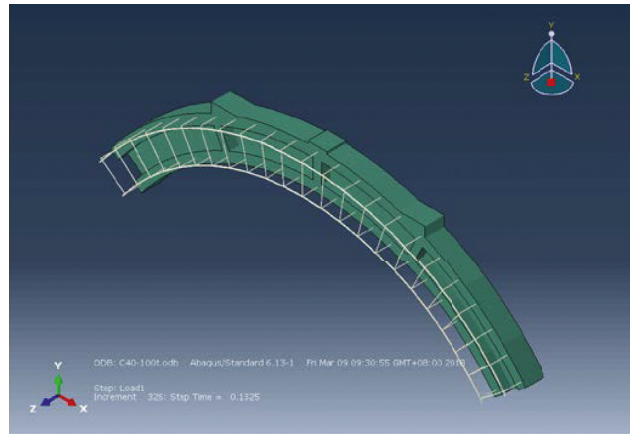

Figure 14: FEM of the UHPFRC arch.

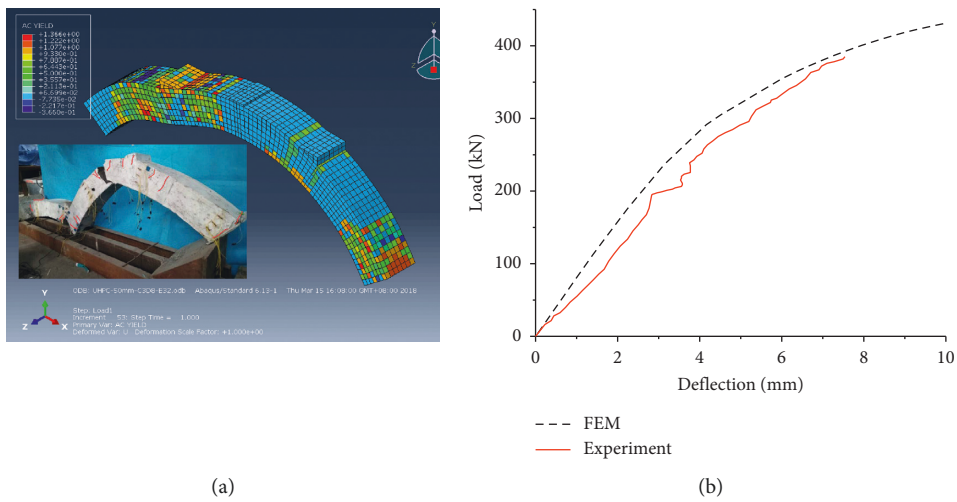

Figure 15: Comparison of experiment and FEM results. (a) Crack pattern. (b) Load-deflection behavior.

From the results of Figure 15, FEM with double nonlinearity had the same failure mode with the experimental arch, and the formation of multihinges was the fracture mode in the UHPFRC arch. The failure load was higher in FEM compared to the experimentally observed failure load (about 87% of FEM result). This difference was derived from constraint conditions and material properties. The constraint of the arch-foot-consolidation is not strong enough in the experiment, but the constraint in FEM is completely confined. The other reason is that the fiber distribution direction and concentration of the materials in the experiment are different from the FEM calculation model.

5. Conclusions

In the present paper, experimental, analytical, and numerical investigations of the thin-walled UHPFRC arch were carried out. Mechanical testing of material properties and columns were conducted in order to determine UHPFRC material properties under compressive force, and these results were used for UHPFRC section design and the numerical modelling. The following conclusions were drawn regarding the outcomes of the study:

(1) Results obtained from the UHPFRC thin-walled column experimental tests indicated that the material utilization rates were influenced by wall thickness and stirrups. The mechanical properties of the UHPFRC sections were stable when thickness was 50 mm and have a reasonable number of stirrups.

(2) In the case of model arches, higher ultimate load and stronger crack limiting ability of UHPFRC arch compared to NC arch was observed. The UHPFRC arch increased the strength and ductile behavior allowing the concrete to deform and support high flexural and compressive force, even after initial cracking. The steel fibers in UHPFRC arch postponed cracks, limited the crack spread, and improved the section stiffness.

(3) The analytical model was able to predict the ultimate load capacity of the UHPFRC arch under concentrated load. The model established by the limit equilibrium method provided an effective way to determine the load capacity for the UHPFRC arch. The results of the FEM indicated the CDP model captured both ultimate load and failure mode of UHPFRC arch with high accuracy.

In this work, combined with the phenomenon of destruction during the test, it can show that the mechanical properties of UHPFRC are between ordinary concrete and steel. The correlation between stability and strength based on size of UHPFRC should be analyzed for further study.

Data Availability

The data used to support the findings of this study are available from the corresponding author upon request.

Conflicts of Interest

The authors declare that there are no conflicts of interests regarding the publication of this paper.

Acknowledgments

The authors acknowledge the support of the National Key Research and Development Program of China (2017YFC0806007), the National Science Fund for Distinguished Young Scholars (51425801), and the National Natural Science Foundation of China (51808081).

References

[1] M. Zhou, W. Lu, J. Song, and G. C. Lee, "Application of ultra-high performance concrete in bridge engineering," *Construction and Building Materials*, vol. 186, pp. 1256–1267, 2018.

[2] X. Shao, M. Qiu, and B. Yan, "A review on the research and application of ultra-high performance concrete in bridge engineering around the world," *Materials Review*, vol. 31, no. 12, pp. 33–43, 2017.

[3] X. Shao and J. Cao, "Fatigue assessment of Steel-UHPC lightweight composite deck based on multiscale FE analysis: case study," *Journal of Bridge Engineering*, vol. 1, no. 1, article 5017015, 2018.

[4] M. Alkaysi and S. El-Tawil, "Effects of variations in the mix constituents of ultra high performance concrete (UHPC) on cost and performance," *Materials and Structures*, vol. 49, no. 10, pp. 4185–4200, 2015.

[5] S. He, Z. Fang, and A. S. Mosallam, "Push-out tests for perfobond strip connectors with UHPC grout in the joints of steel-concrete hybrid bridge girders," *Engineering Structures*, vol. 135, pp. 177–190, 2017.

[6] M. Tazarv and M. S. Saiidi, "UHPC-filled duct connections for accelerated bridge construction of RC columns in high seismic zones," *Engineering Structures*, vol. 99, pp. 413–422, 2015.

[7] A. Meda, S. Mostosi, Z. Rinaldi, and P. Riva, "Corroded RC columns repair and strengthening with high performance fiber reinforced concrete jacket," *Materials and Structures*, vol. 49, no. 5, pp. 1967–1978, 2015.

[8] I. H. Yang, C. Joh, and B.-S. Kim, "Structural behavior of ultra high performance concrete beams subjected to bending," *Engineering Structures*, vol. 32, no. 11, pp. 3478–3487, 2010.

[9] D.-Y. Yoo and Y.-S. Yoon, "Structural performance of ultra-high-performance concrete beams with different steel fibers," *Engineering Structures*, vol. 102, pp. 409–423, 2015.

[10] S. Ghasemi, P. Zohrevand, A. Mirmiran, Y. Xiao, and K. Mackie, "A super lightweight UHPC-HSS deck panel for movable bridges," *Engineering Structures*, vol. 113, pp. 186–193, 2016.

[11] J. Xia, K. R. Mackie, M. A. Saleem, and A. Mirmiran, "Shear failure analysis on ultra-high performance concrete beams reinforced with high strength steel," *Engineering Structures*, vol. 33, no. 12, pp. 3597–3609, 2011.

[12] M. A. Al-Osta, M. N. Isa, M. H. Baluch, and M. K. Rahman, "Flexural behavior of reinforced concrete beams strengthened with ultra-high performance fiber reinforced concrete," *Construction and Building Materials*, vol. 134, pp. 279–296, 2017.

[13] P. R. Prem, A. R. Murthy, and M. Verma, "Theoretical modelling and acoustic emission monitoring of RC beams strengthened with UHPC," *Construction and Building Materials*, vol. 158, pp. 670–682, 2018.

[14] A. P. Lampropoulos, S. A. Paschalis, O. T. Tsioulou, and S. E. Dritsos, "Strengthening of reinforced concrete beams using ultra high performance fibre reinforced concrete (UHPFRC)," *Engineering Structures*, vol. 106, pp. 370–384, 2016.

[15] J. Li, C. Wu, H. Hao, and Z. Liu, "Post-blast capacity of ultra-high performance concrete columns," *Engineering Structures*, vol. 134, pp. 289–302, 2017.

[16] A. R. Malik and S. J. Foster, "Behaviour of reactive powder concrete columns without steel ties," *Journal of Advanced Concrete Technology*, vol. 6, no. 2, pp. 377–386, 2008.

[17] C. Shi, M. Long, C. Cao, G. Long, and M. Lei, "Mechanical property test and analytical method for Reactive Powder Concrete columns under eccentric compression," *KSCE Journal of Civil Engineering*, vol. 21, no. 4, pp. 1307–1318, 2016.

[18] C.-C. Hung, F.-Y. Hu, and C.-H. Yen, "Behavior of slender UHPC columns under eccentric loading," *Engineering Structures*, vol. 174, pp. 701–711, 2018.

[19] M. N. S. Hadi and A. Al-Tikrite, "Behaviour of fibre-reinforced RPC columns under different loading conditions," *Construction and Building Materials*, vol. 156, pp. 293–306, 2017.

[20] B. Shan, D.-D. Lai, Y. Xiao, and X.-B. Luo, "Experimental research on concrete-filled RPC tubes under axial compression load," *Engineering Structures*, vol. 155, pp. 358–370, 2018.

[21] T. Makita and E. Brühwiler, "Tensile fatigue behaviour of ultra-high performance fibre reinforced concrete (UHPFRC)," *Materials and Structures*, vol. 47, no. 3, pp. 475–491, 2013.

[22] Z. Zheng, S. Zhang, and D. Peng, "Experimental study on ultimate strength of reinforced concrete arch," *Journal of Fuzhou University*, no. 2, pp. 79–90, 1982.

[23] L. Hussein and L. Amleh, "Structural behavior of ultra-high performance fiber reinforced concrete-normal strength concrete or high strength concrete composite members," *Construction and Building Materials*, vol. 93, pp. 1105–1116, 2015.

[24] S. AFGC, *Ultra High Performance Fibre Reinforced Concretes, Recommendations*, AFGC and SETRA Working Group, Paris, France, 2013.

[25] N. G. R. Gowripalan, *Design Guidelines for Ductal Prestressed Concrete Beams*, School of Civil and Environmental Engineering, the University of NSW, Sydney, Australia, 2000.

[26] JSCE JSOC, *Recommendations for Design and Construction of High Performance Fiber Reinforced Cement Composites with Multiple Fine Cracks (HPFRCC)*, Concrete Committee-Concrete Engineering Series, Tokyo, China, 2008.

[27] S. Aaleti, B. Petersen, and S. Sritharan, *Design Guide for Precast UHPC Waffle Deck Panel System, Including Connections*, Federal Highway Administration, Washington, DC, USA, 2013.

[28] B. A. Graybeal, *Structural Behavior of Ultra-High Performance Concrete Prestressed I-Girders*, Federal Highway Administration, Mclean, VA, USA, 2006.

[29] B. A. Graybeal, *Material Property Characterization of Ultra-High Performance Concrete*, Federal Highway Administration, Mclean, VA, USA, 2006.